IEEE Access
Multidisciplinary | Rapid Review | Open Access Journal

Received October 30, 2020, accepted November 8, 2020, date of publication November 16, 2020, date of current version November 20, 2020.

Digital Object Identifier 10.1109/ACCESS.2020.3037778

Slots-Coupled Omnidirectional Circularly Polarized Cylindrical Glass Dielectric Resonator Antenna for 5.8-GHz WLAN Application

XIAO SHENG FANG[1,3], (Member, IEEE),
LING PENG WENG[1,3], (Graduate Student Member, IEEE),
AND YU-XIANG SUN[2], (Member, IEEE)

[1]Department of Electronic and Information Engineering, Shantou University, Shantou 515063, China
[2]College of Electronics and Information Engineering, Shenzhen University, Shenzhen 518060, China
[3]Guangdong Provincial Key Laboratory of Digital Signal and Image Processing, Shantou University, Shantou 515063, China

Corresponding author: Xiao Sheng Fang (fangxs@stu.edu.cn)

This work was supported in part by the National Natural Science Foundation of China under Grant 61701292 and Grant 62001306, in part by the Department of Education of Guangdong Province under Grant 2020ZDZX3015, in part by the Department of Science and Technology of Guangdong Province under Grant 2020A1414010366, and in part by the Natural Science Foundation of Shenzhen University under Grant 2019008.

ABSTRACT In this paper, a slots-coupled omnidirectional circularly polarized (CP) cylindrical dielectric resonator antenna (DRA) is proposed. The $TM_{01\delta}$ and $TE_{011+\delta}$ modes of the cylindrical DRA are simultaneously excited by four printed slots placed at 45 degrees to the radial direction. Omnidirectional CP fields are obtained when the fields of the two modes have the same amplitude and 90 degrees phase difference. Compared with the traditional probe-fed method, the structure of the proposed slots-coupled DRA is very simple, without introducing any groove, patch, choke or shorting pins. For the demonstration, a slots-coupled omnidirectional CP cylindrical glass DRA is designed for 5.8-GHz WLAN application. It is found that the proposed DRA can provide an AR bandwidth of ∼8 % (5.62-6.09 GHz) and a gain of ∼5.6 dBic, with a height of $\sim 0.127\lambda_0$. This performance is competitive with other reported omnidirectional CP DRAs.

INDEX TERMS Cylindrical dielectric resonator antenna, slots-coupled, omnidirectional, circularly polarized.

I. INTRODUCTION

In the last three decades, dielectric resonator antenna (DRA) [1]–[4] has been widely investigated owning to its small volume, easy excitation and controllable bandwidth. Recently, DRA fabricated using K9 glass [5]–[7] has received more and more attention. Compared with the traditional DRA, glass DRA has a transparent appearance, which makes it possible to be a multifunctional microwave devices. Related work such as glass DRA used as a mirror [5], socket [6] and light cover [7] have been reported.

For indoor communication, an omnidirectional antenna is usually preferred since it can cover a larger area. On the other hand, circularly polarized (CP) antenna is very popular since it allows more flexible orientation between the transmitter and receiver. Also, it can suppress multi-path interference. Consequently, some omnidirectional CP DRAs [8]–[14] have been studied. For example, an omnidirectional CP rectangular DRA [8] was successfully achieved by introducing inclined grooves to the sidewalls of the DRA. In this example, the inclined grooves are used to excite a degenerate mode for the generation of CP fields. In [9], an omnidirectional CP cylindrical DRA loading with an Alford-loop patch is investigated. By combining electrical-dipole TM-mode of the DRA and magnetic-dipole mode of the conducting loop, CP fields can be obtained. Similarly, another omnidirectional CP cylindrical DRA [10] is achieved by using TM-mode of the DR and slotted ground plane. In this example, a choke is needed to reduce the back radiation of the slots. All the above work on omnidirectional CP DRAs [8]–[14] is using axial probe feeding. However, this method has several disadvantages. Firstly, it is required to drill a hole into the DRA for accommodating the probe, and thus it increases the difficulty of the DRA fabrication. Secondly, supplementary technique

The associate editor coordinating the review of this manuscript and approving it for publication was Shah Nawaz Burokur.

like grooves [8], patch [9] or choke [10] is required for generating an omnidirectional CP fields, which would increase the complexity of the design. Finally, probe-fed method is relatively difficult to excite the low-height DRA (please refer to Fig.21).

To avoid hole-drilling in DRA, planar-fed method is studied. For example, an omnidirectional CP DRA fed by a planar microstrip cross is proposed in [15]. In this method, the $TM_{01\delta}$ and $TE_{011+\delta}$ modes of the cylindrical DRA are used to design the CP DRA. The former one is excited by a patch placed at center of the DRA, while the latter one is excited by four microstrip arcs. The disadvantage is that it requires the shorting pins to reduce the size of the planar microstrip cross.

The slot-coupled method has been widely employed to design the CP DRA with broadside radiation pattern [16]–[20], but rarely used to excite the omnidirectional CP DRA. In this article, this method is applied to design the omnidirectional CP cylindrical DRA. The $TM_{01\delta}$ and $TE_{011+\delta}$ modes of the cylindrical DRA are excited by four printed slots, which are placed at 45 degrees to the radial direction. Omnidirectional CP fields are achieved as the fields of the two modes have same amplitude and 90° phase difference. With this method, omnidirectional CP DRA can be achieved without the need to introduce inclined groove, patch, planar choke or shorting pin, making the design very simple. In addition, no hole drilling in the DR is needed. This feature is very suitable for designing glass DRA since drilling hole is easy to make the glass brittle. For the demonstration, an omnidirectional CP cylindrical glass DRA is designed for 5.8-GHz WLAN application. The reflection coefficient, axial ratio (AR), radiation pattern and antenna gain are studied by ANSYS HFSS. A prototype is fabricated and measurements were carried out for verification. Reasonable agreement between the simulation and measurement is obtained.

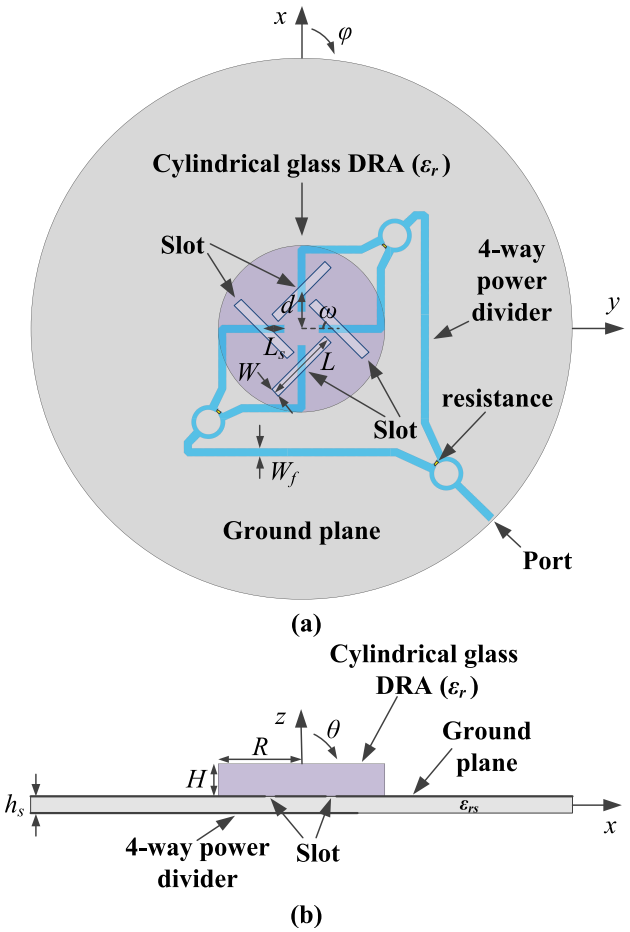

FIGURE 1. The geometry of the slots-coupled omnidirectional CP cylindrical DRA. (a) Top view. (b) Side view. $\varepsilon_r = 6.85$, $R = 20$ mm, $H = 6.5$ mm, $L = 19$ mm, $W = 2.2$ mm, $d = 9$ mm, $\varepsilon_{rs} = 2.94$, $h_s = 0.762$ mm, $W_f = 1.94$ mm and $L_s = 5$ mm.

II. ANTENNA GEOMETRY, WORKING PRINCIPLE AND PARAMETRIC STUDY

A. ANTENNA GEOMETRY

The geometry of the slots-coupled omnidirectional CP glass cylindrical DRA is shown in Fig. 1. The cylindrical DRA has a dielectric constant of $\varepsilon_r = 6.85$, a radius of $R = 20$ mm and a height of $H = 6.5$ mm ($H/R = 0.325$). Using the formulas (A1) and (A2) in Appendix, the resonance frequencies of the $TM_{01\delta}$ and $TE_{011+\delta}$ modes of the DRA are estimated as 5.63 GHz and 5.91 GHz, respectively. To excite an omnidirectional CP DRA, the slots having an angle of $\omega = 45°$ with respective to the radial direction are needed. Each slot has a length of $L = 19$ mm and a width of $W = 2.2$ mm, with a distance of $d = 9$ mm from the origin. The slots are printed on a ground plane of a circular substrate, which has a dielectric constant of $\varepsilon_{rs} = 2.94$, a thickness of $h_s = 0.762$ mm and a diameter of 130 mm. To provide in-phased signals for the slots, a 4-way power divider ($W_f = 1.94$ mm, $L_s = 5$ mm) operating around 5.8 GHz was designed on the bottom side of the substrate.

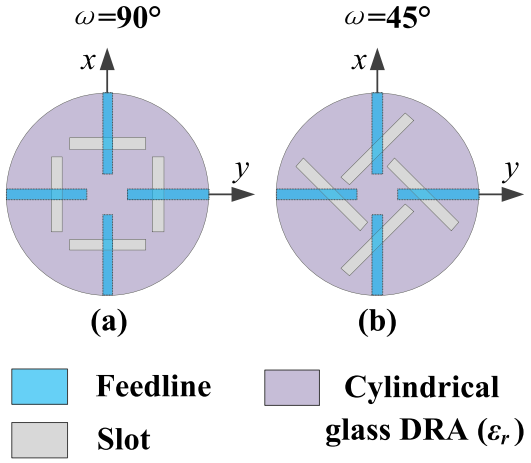

FIGURE 2. Simplified configuration of the slots-coupled cylindrical DRA. (a) $\omega = 90°$. (b) $\omega = 45°$.

B. WORKING PRINCIPLE

1. The working principle of the proposed DRA is studied here. Two cases of $\omega = 90°$ and $\omega = 45°$ are discussed, with their

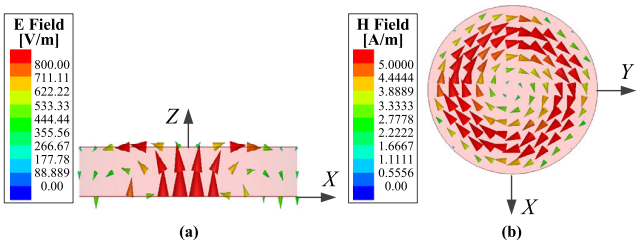

FIGURE 3. Simulated E-and H-fields inside the cylindrical DRA at 5.8 GHz when $\omega = 90°$. (a) E field (x-z plane); (b) H field (x-y plane). The configuration is the same as in Fig. 2 (a).

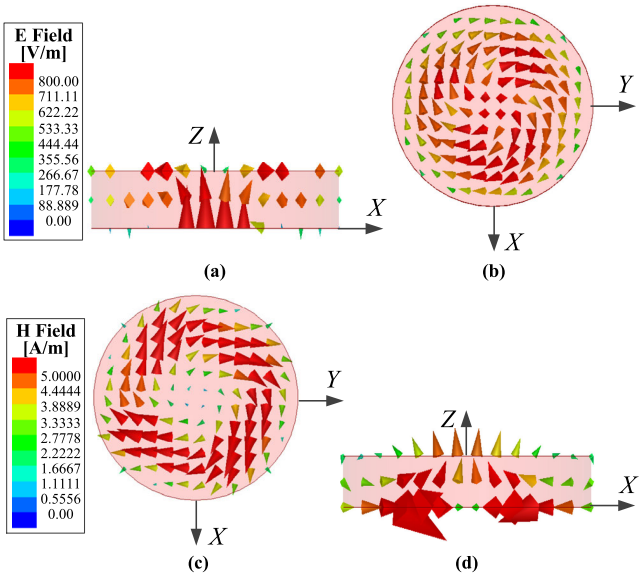

FIGURE 4. Simulated E-and H-fields inside the cylindrical DRA at 5.8 GHz when $\omega = 45°$. (a) E field (x-z plane) at t = 0; (b) E field (x-y plane) at t = $T/4$; (c) H field (x-y plane) at t = $T/4$; (d) H field (x-z plane) at t = $T/2$, in which T denotes the period of time. The configuration is the same as in Fig. 2 (b).

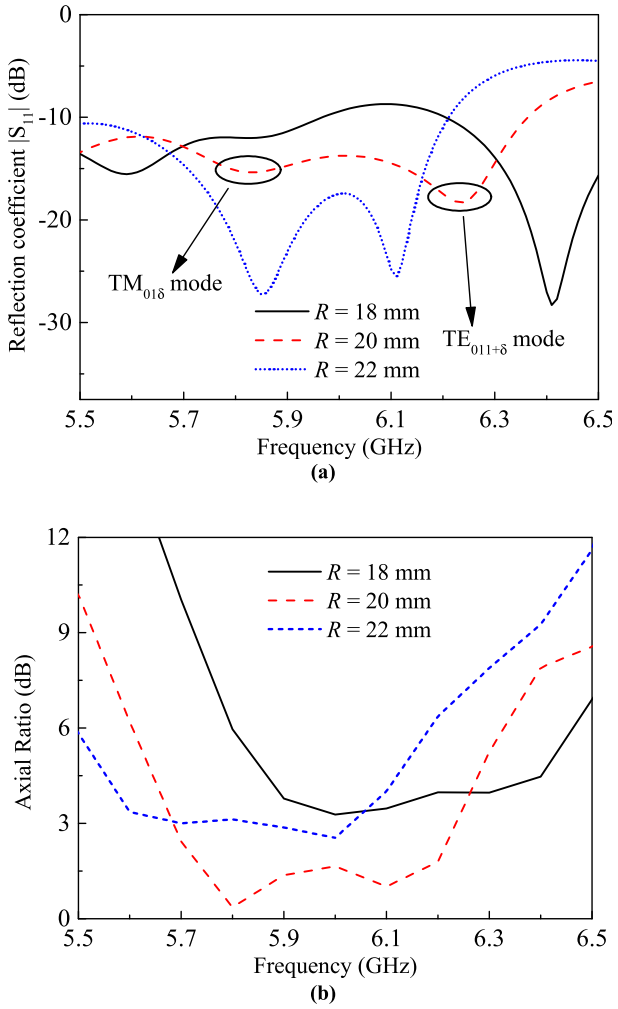

FIGURE 5. Simulated reflection coefficients and ARs of the omnidirectional CP DRA for different R. (a) reflection coefficient. (b) AR ($\theta = 45°$ and $\phi = 0°$).

simplified configuration shown in Fig. 2 (a) and Fig. 2 (b), respectively. Fig. 3 shows the simulated E-and H-fields inside the cylindrical DRA at 5.8 GHz when $\omega = 90°$. As can be seen from the figure, typical $TM_{01\delta}$-mode of the cylindrical DRA is observed. In this case, only omnidirectional linearly polarized (LP) fields are obtained. Fig. 4 presents the simulated E-and H-fields inside the cylindrical DRA at 5.8 GHz when $\omega = 45°$. The fields in (a) and (c) are caused by the $TM_{01\delta}$ mode of the DR, while those in (b) and (d) are due to the $TE_{011+\delta}$ mode of the DR. With reference to Fig. 4 (a) and (b), the two E fields at t = 0 and t = $T/4$ are orthogonal and in phase quadrature, which can produce omnidirectional CP fields. Similarly, as can be seen from Fig. 4 (c) and (d), two H fields at t = $T/4$ and $T/2$ are orthogonal and have a 90° phase difference. As a result, omnidirectional CP fields can be generated. Some design experience is given here. When $0° < \omega < 90°$, the E-field of the slots can be decomposed into the E_θ and E_Φ. The E_θ component is responsible for exciting the $TM_{01\delta}$ mode, while the E_Φ component is used to excite the $TE_{011+\delta}$ mode. Since ω can be used to control these two components, and thus indirectly adjust the amplitude and phase of the $TM_{01\delta}$ and $TE_{011+\delta}$ modes. More design experience will be presented in Fig. 8. In addition, the resonance frequencies of the $TM_{01\delta}$ and $TE_{011+\delta}$ modes should be close enough to generate the CP fields in the design.

C. PARAMETRIC STUDY

The proposed design is target for the WLAN-5.8 GHz application. In general, its minimum requirements include: 1). The frequency band covers 5.725-5.85GHz; 2). The antenna gain is greater than 5dBic; 3). The radiation pattern of the antenna is omnidirectional. Parametric study is carried out to study and optimize the proposed DRA in this section. Fig. 5 (a) shows the simulated reflection coefficients versus frequency with $R = 18$ mm, 20 mm and 22 mm. As can be found from the figure, the two resonant modes are excited at 5.85 GHz and 6.21 GHz when $R = 20$ mm, respectively, which are due to the $TM_{01\delta}$ and $TE_{011+\delta}$ modes, with their estimated values of 5.63 GHz (3.9% error) and 5.91 GHz (5 % error) mentioned in section A. It can be found that changing R

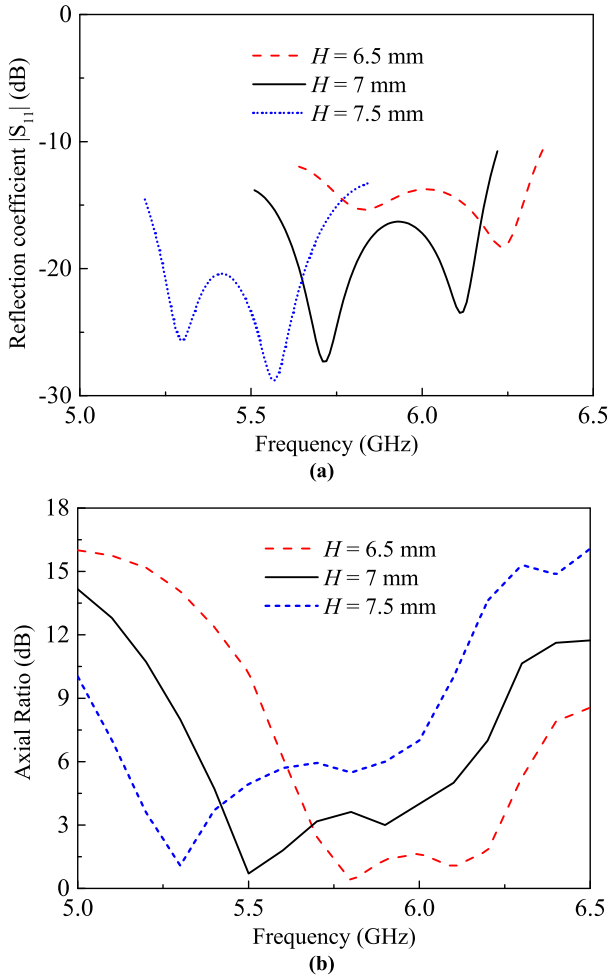

FIGURE 6. Simulated reflection coefficients and ARs of the omnidirectional CP DRA for different *H*. (a) reflection coefficient. (b) AR ($\theta = 45°$ and $\phi = 0°$).

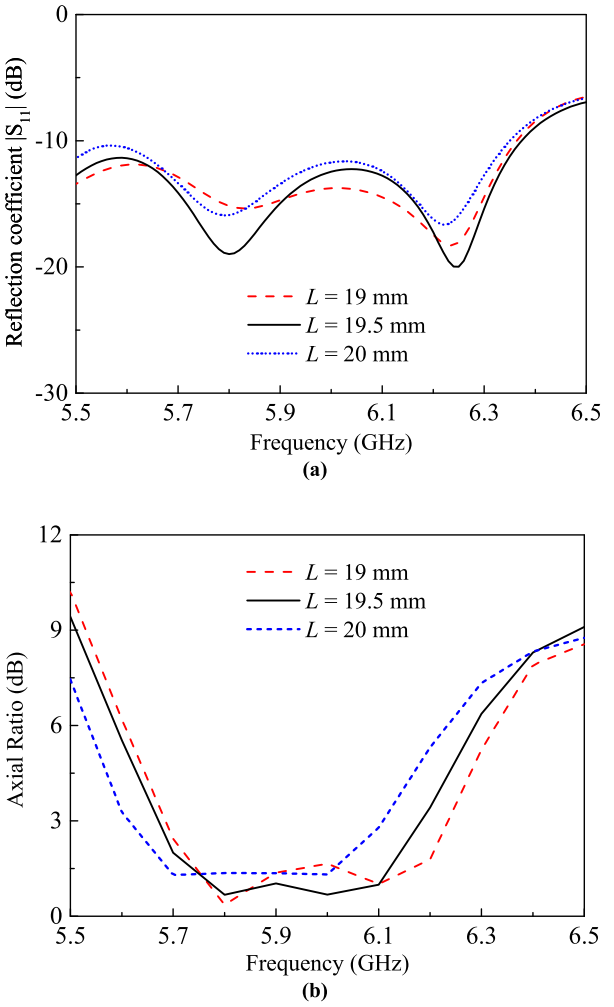

FIGURE 7. Simulated reflection coefficients and ARs of the omnidirectional CP DRA for different *L*. (a) reflection coefficient. (b) AR ($\theta = 45°$ and $\phi = 0°$).

has a relatively large effect on the reflection coefficient of the DRA. Fig. 5 (b) shows the corresponding ARs ($\theta = 45°$ and $\phi = 0°$) versus frequency. Similarly, altering R will affect the AR obviously. Fig. 6 (a) and (b) show the simulated reflection coefficients and ARs versus frequency with $H = 6.5$ mm, 7 mm and 7.5 mm, respectively. It can be found from the figures that changing H would shift the resonance modes obviously, verifying the resonance modes are dominated by the DRA. Fig. 7 (a) and (b) show the simulated reflection coefficients and corresponding ARs versus frequency with the slot length $L = 19$ mm, 19.5 mm and 20 mm. Referring to the figure, changing L has a relatively small effect on the reflection coefficient and AR of the DRA. The above results show that the excited resonant modes are dominated by the DRA but not slots.

Fig. 8 (a) and (b) show the simulated reflection coefficients and corresponding ARs versus frequency with $\omega = 30°$, 45° and 60°, respectively. Referring to Fig. 8, the levels of the reflection coefficient and AR are significantly changed by altering the angle ω. Fig. 9 (a) and (b) show the simulated reflection coefficients and corresponding ARs versus frequency with different d. Referring to the figure, changing d can change the AR without affecting the matching obviously. This provides an optimization direction. The matching of the DRA can be adjusted firstly by the angle ω, then a good AR can be obtained by adjusting d.

D. POWER DIVIDER

It is interesting to study the effect of the resistor (r) of the power divider. Fig. 10 presents the simulated reflection coefficients and corresponding ARs when $r = 50\ \Omega$, $100\ \Omega$ and left open. With reference to the figure, the results without and with resistor are almost the same. The radiation pattern and antenna gain have also been studied for the two cases, and the results are almost the same. This shows that the resistor has little impact on the performance of the DRA. It is reasonable because the potentials at both ends of the isolation resistors are equal when port 2, 3, 4 and 5 (Figure 11) are matched. This indicates no current flows through the resistors, and therefore the resistors can be ignored.

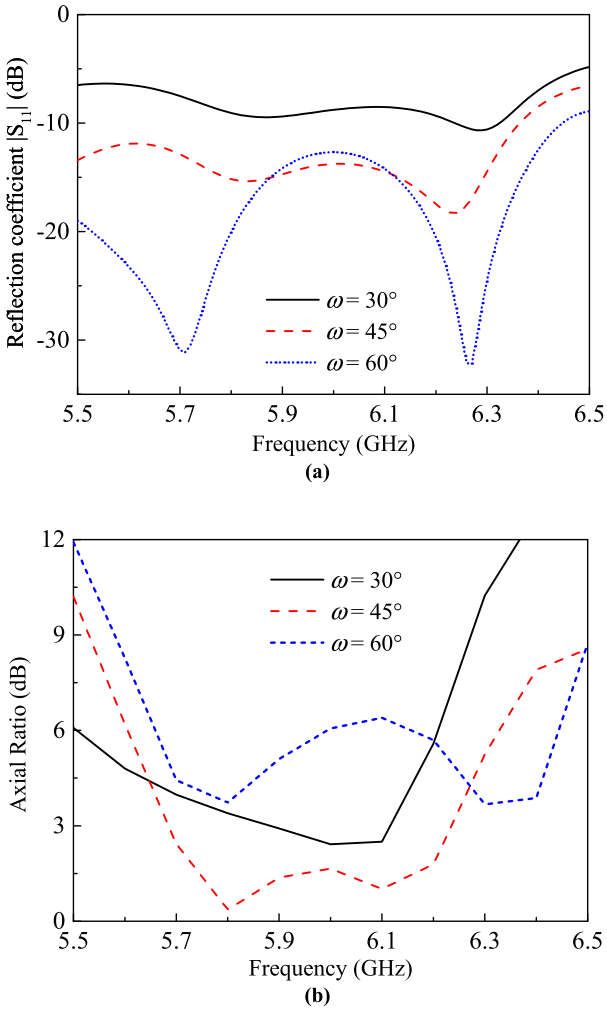

FIGURE 8. Simulated reflection coefficients and ARs of the omnidirectional CP DRA for different ω. (a) reflection coefficient. (b) AR ($\theta = 45°$ and $\phi = 0°$).

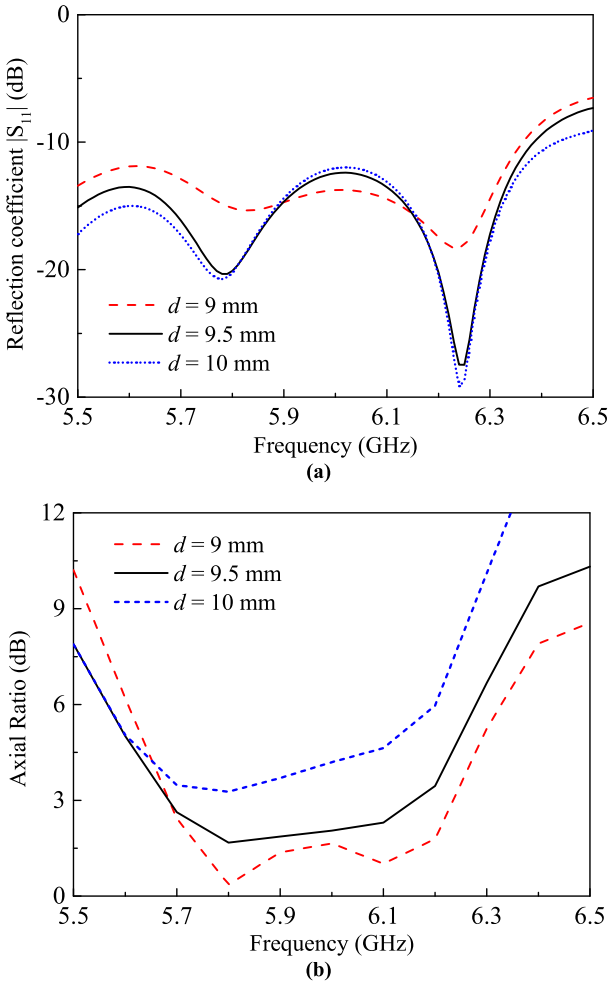

FIGURE 9. Simulated reflection coefficients and ARs of the omnidirectional CP DRA for different d. (a) reflection coefficient. (b) AR ($\theta = 45°$ and $\phi = 0°$).

To further verify the above viewpoint, the performance of the 4-way power divider without resistor is studied. Fig. 11 shows the simplified configuration of the power divider, which consists of two stages of the Wilkinson power divider. Its input port is labeled as port 1, while its output ports are labeled as port 2, 3, 4 and 5, respectively. Fig. 12 shows the simulated S parameters of the 4-way power divider. Referring to $|S_{11}|$ in the figure, good match is obtained across the frequency band (5.5- 6.5 GHz). The working frequency of the power divider is observed as 5.93 GHz, which agrees well with the designed value of 5.8 GHz (2.24% error). In addition, the outputs of the power divider ($|S_{21}|$, $|S_{31}|$, $|S_{41}|$ and $|S_{51}|$) satisfy the requirement of ($|S| < 6 \pm 1$dB) across the frequency band, indicating the amplitude of four output signals are almost the same. Fig. 13 shows the simulated phase difference between port 2 and port 3, 4, 5, respectively. The results satisfy the requirement of ($0° \pm 2°$) over the frequency band (5.5 - 6.5 GHz). The above research shows that the power divider without resistor can still provide in-phased output signals with the same amplitude. It should be mentioned that the mutual coupling of the power divider degrades when the resistors are removed from the power divider. The analysis of the mutual coupling is required when the system exists a amount of reflected wave. In our case, no or very small reflected wave was produced as the output ports are matched. Therefore, the degrade of the mutual coupling (without resistor) do not have a large effect on the performance of the antenna.

E. COMPARISON OF DRA WITH DIFFERENT SHAPES

In this section, the performance of the slots-coupled DRAs of different shapes is compared. Three common shapes are chosen, including the cylindrical, rectangular and equilateral triangular. Both the rectangular and triangular DRAs ($\varepsilon_r = 6.85$) have the same base area and height as the cylindrical one (Fig. 1). Fig. 14 (a) and (b) show their simulated reflection coefficients and ARs, respectively. Referring to the figure, three DRAs have a good matching and AR ($\theta = 45°$ and $\phi = 0°$) nearby 5.8 GHz, in which the cylindrical DRA has a largest AR bandwidth. The RHCP

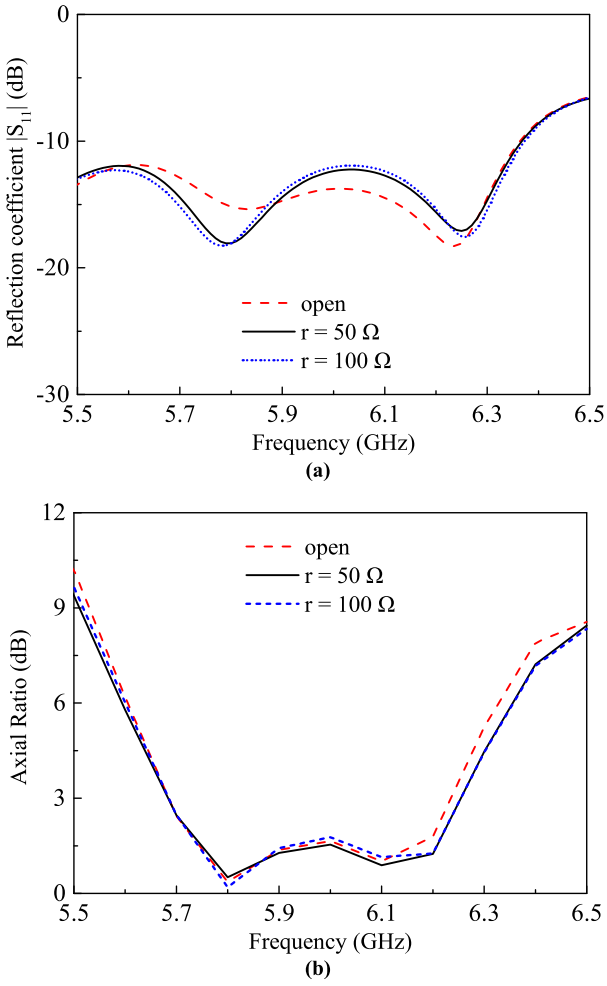

FIGURE 10. Simulated reflection coefficients and ARs of the omnidirectional CP DRA for different values of resistor r. (a) reflection coefficient. (b) AR ($\theta = 45°$ and $\phi = 0°$).

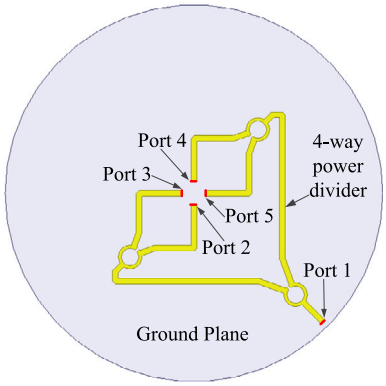

FIGURE 11. The top view of the 4-way power divider without the resistor.

patterns in azimuth plane of the three DRAs are also studied in Fig. 15. It can be observed from the figure that the field fluctuations of the cylindrical, rectangular and triangular DRAs are 1.26, 1.67 and 12.31 dB, respectively, indicating the omnidirectional property of the cylindrical one is best.

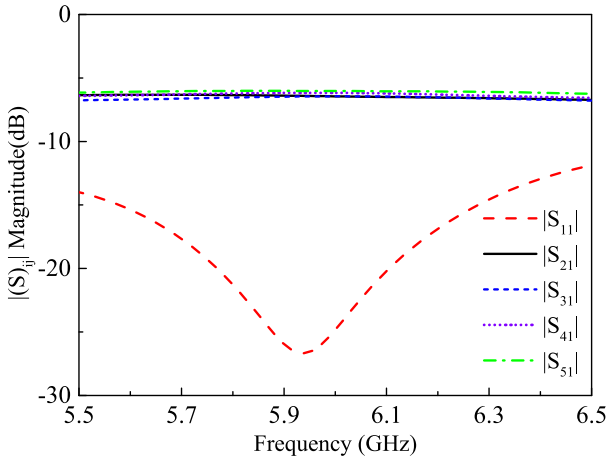

FIGURE 12. Simulated S parameters of the power divider.

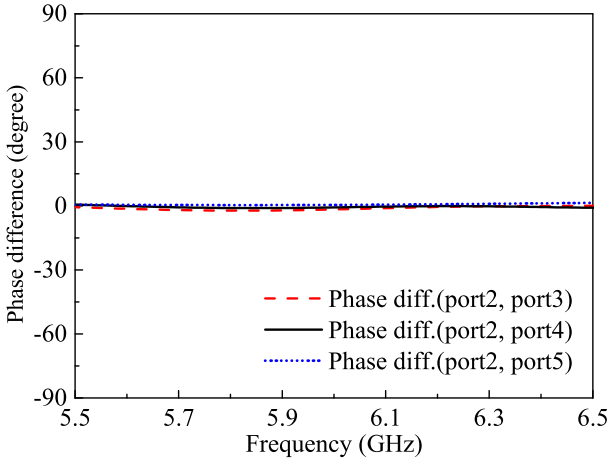

FIGURE 13. Simulated phase difference between four output ports of the power divider.

The above analysis show that the cylindrical one which has symmetrically rotational shape in azimuth plane is more suitable for the design.

III. RESULTS

In this part, the performance of the proposed DRA is shown. Fig. 16 shows the prototype of the omnidirectional CP cylindrical DRA fabricated by using transparent K9 glass. It can be seen from the figure that the design only consists of a solid glass cylindrical DRA and a substrate, which is very simple. Fig. 17 presents the measured and simulated reflection coefficients of the proposed omnidirectional CP cylindrical DRA. Reasonable agreement between the simulated and measured results is obtained. The measured impedance bandwidth ($|S_{11}| \leqslant -10$ dB) is obtained as 13.7 % (5.5–6.31 GHz). Fig. 18 shows the measured and simulated ARs ($\theta = 45°$ and $\phi = 0°$) of the proposed DRA. The measured 3-dB AR bandwidth is ∼8 % (5.62-6.09 GHz), covering the whole 5.8 GHz WLAN band. It should be mentioned that the measured AR

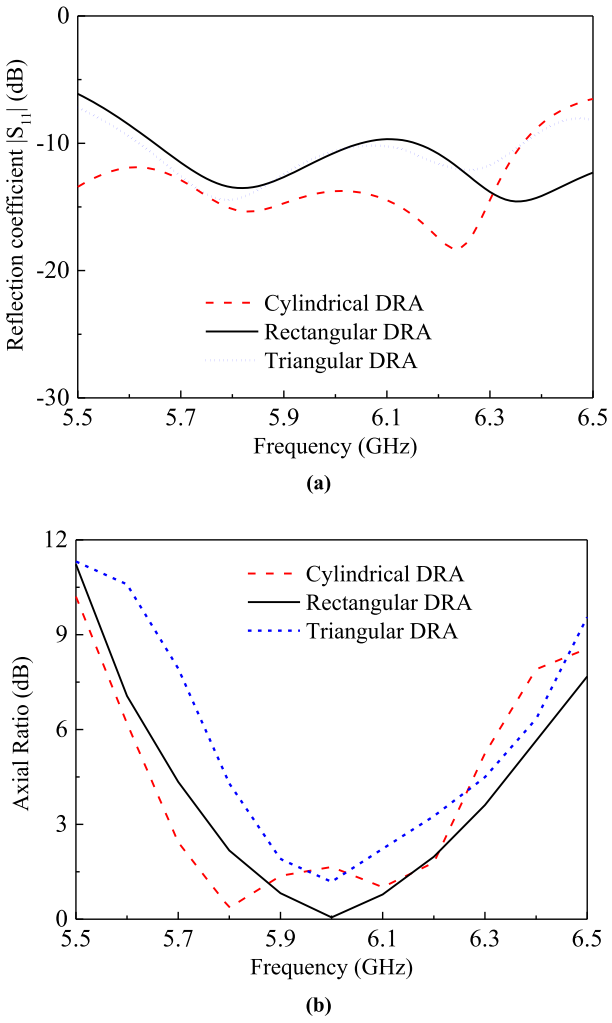

FIGURE 14. Simulated reflection coefficients and ARs of the DRA with different shapes: cylindrical, rectangular and triangular. (a) Reflection coefficient. (b) AR ($\theta = 45°$ and $\phi = 0°$).

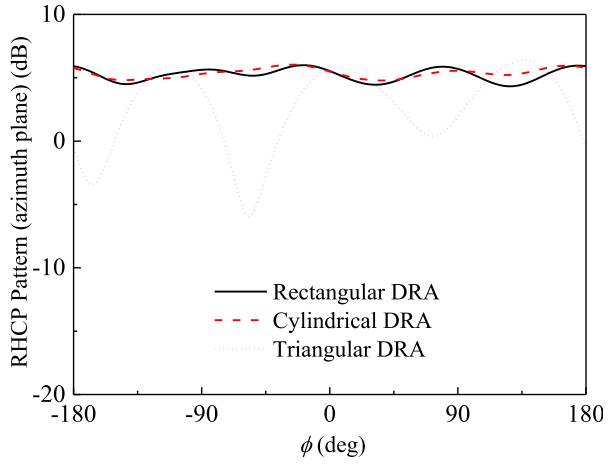

FIGURE 15. Simulated RHCP patterns in azimuth plane ($\theta = 45°$) of the DRA with different shapes: cylindrical (5.8 GHz), rectangular (6.0 GHz) and triangular (6.0 GHz).

passband completely falls within its respective impedance passband, therefore the entire AR bandwidth is usable.

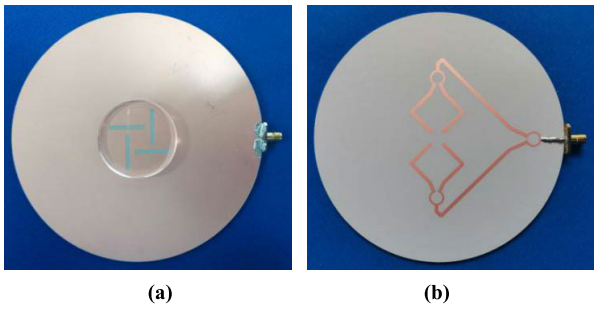

FIGURE 16. The prototype of the slots-coupled omnidirectional CP cylindrical glass DRA. (a) Front side. (b) Bottom side.

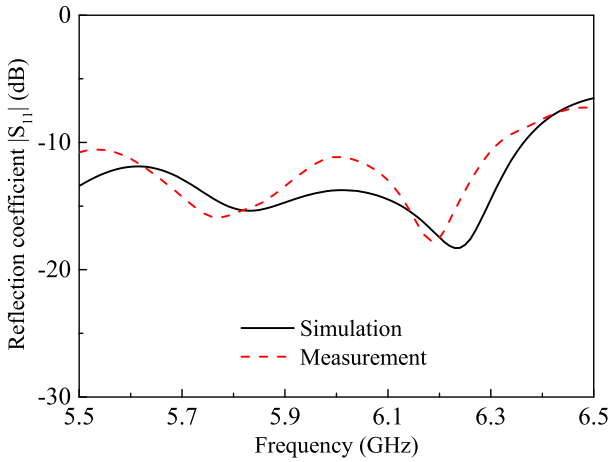

FIGURE 17. Measured and simulated reflection coefficients of the proposed slots-coupled omnidirectional CP cylindrical DRA versus frequency.

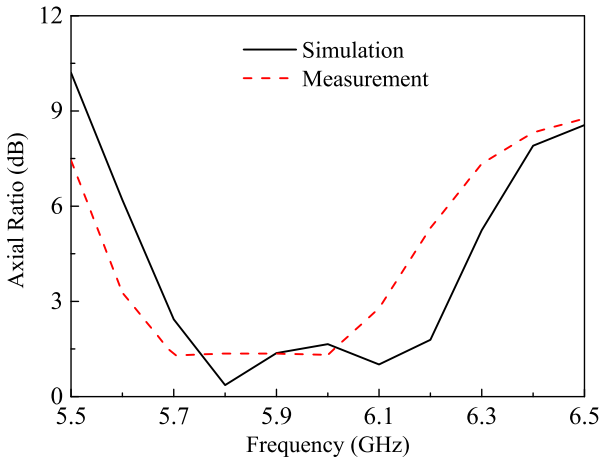

FIGURE 18. Measured and simulated ARs ($\theta = 45°$ and $\phi = 0°$) of the proposed slots-coupled omnidirectional CP cylindrical DRA versus frequency.

Satimo StarLab system is employed to do the far-field measurement. Fig. 19 shows the simulated and measured radiation patterns in the elevation plane (x-z plane) and azimuth plane ($\theta = 45°$) at 5.8 GHz and 6.05 GHz, respectively. With reference to the figure, omnidirectional pattern dominated by

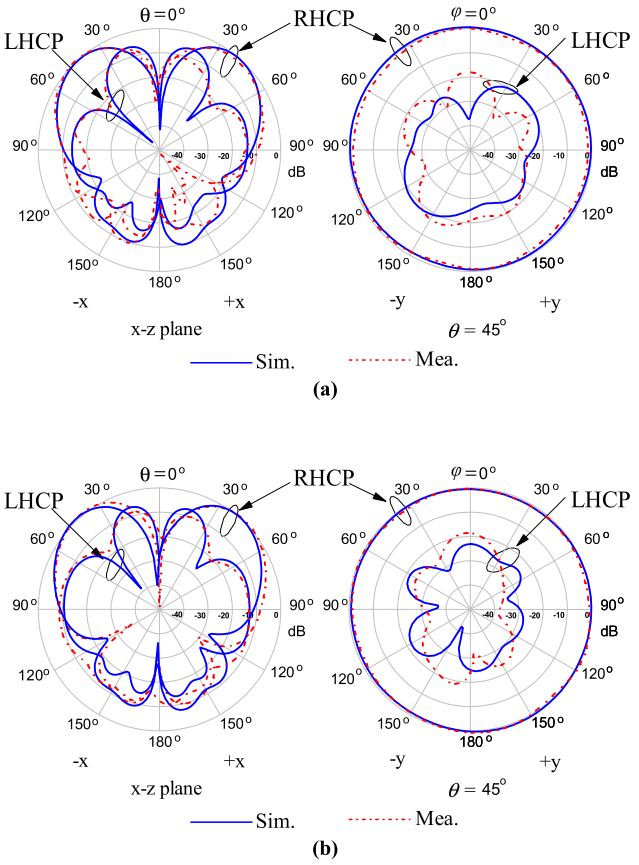

FIGURE 19. Measured and simulated radiation patterns of the proposed slots-coupled omnidirectional CP cylindrical DRA. (a) 5.8 GHz. (b) 6.05 GHz.

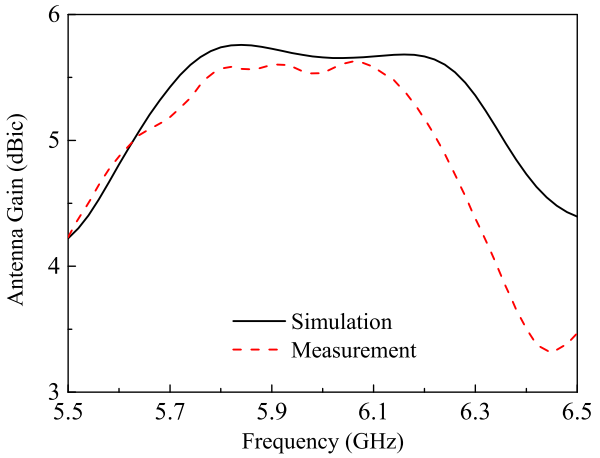

FIGURE 20. Measured and simulated antenna gains of the proposed slots-coupled omnidirectional CP cylindrical DRA versus frequency.

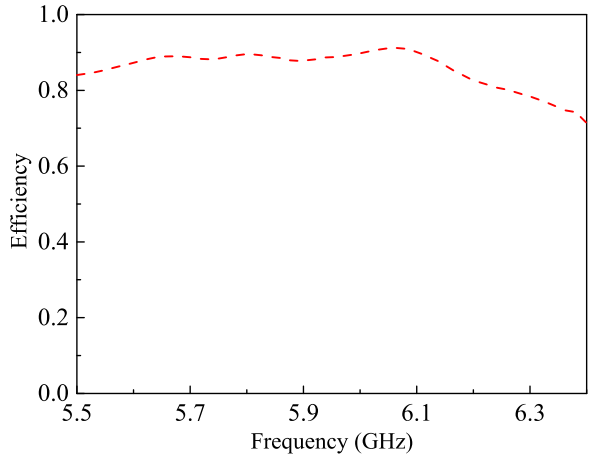

FIGURE 21. Measured efficiency of the proposed DRA versus frequency.

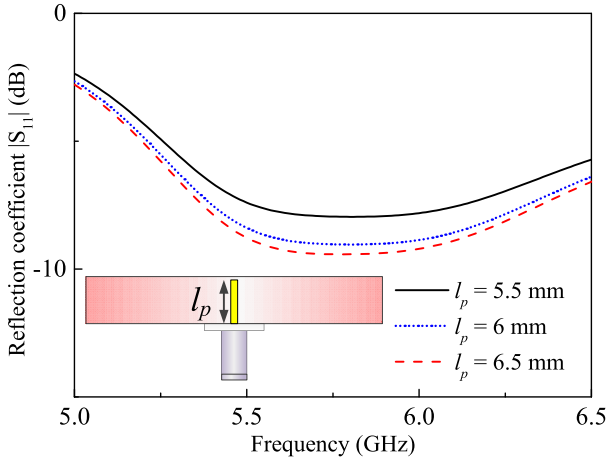

FIGURE 22. Simulated reflection coefficients of the cylindrical DRA fed by a conducting probe with different probe length l_p.

the RHCP fields is observed. The RHCP fields are stronger than the LHCP fields by more than 18 dB at arbitrary angles in the azimuth plane. The elevation pattern has a tilting angle at $\theta = 45°$, which is caused by the effect of a ground plane. Radiation patterns at other frequencies have also been studied, and it was found that the DRA shows a stable omnidirectional CP pattern across the whole frequency band. Fig. 20 presents the measured and simulated antenna gains of the proposed DRA, with $\theta = 45°$ and $\phi = 0°$. Referring to the figure, the measured peak gain was observed as 5.6 dBic at 5.9 GHz. It is worth mentioning that the higher antenna gain of the proposed DRA is mainly due to a large ground plane, which has a diameter of $2.5\lambda_0$. The performance of the proposed DRA satisfies the minimum requirements mentioned in Section C of the Part II. The measured efficiency of the proposed DRA is also given in Fig. 21. With reference to the figure, It ranges from 0.88 to 0.91 across the usable frequency band (5.62 - 6.09 GHz).

Finally, the performance of the proposed slots-coupled omnidirectional CP cylindrical DRA is assessed. Firstly, a reference probe-fed cylindrical DRA having the same dielectric constant and dimension with that in Fig.1 was investigated, with its simulated reflection coefficient shown in Fig. 22. With reference to the figure, the cylindrical DRA can not be well excited using the probe-fed method. This is because the limited height of DRA restricts the probe length, making it difficult to obtain a good matching. In other words,

TABLE 1. Comparison of the different omnidirectional CP DRAs.

Ref.	Shape	ε_r	Size (λ_d^3)	Height (H/λ_0)	Radius (R/λ_0)	Length (a/λ_0)	Width (b/λ_0)	10dB impedance bandwidth (%)	3dB-AR bandwidth (%)	Peak gain (dBic)	Feeding method
[8]	Rectangular	15	1.70	0.276	-	0.326	0.326	24.4	7.3	1.6	probe
[9]	Cylindrical	10	0.66	0.18	0.2	-	-	8.8	4.9	1.8	probe
[10]	Cylindrical	6.85	0.58	0.162	0.25	-	-	8.6	6.2	0.7	probe
[11]	Rectangular	6.85	1.23	0.362	-	0.434	0.434	6.6	6.9	2.11	probe
[12]	Rectangular	10	3.92	0.329	-	0.543	0.543	2.5	4	2.13	probe
[13]	Cylindrical	6.85	0.68	0.203	0.237	-	-	18.0	5.1	1	probe
[14]	Rectangular	15	2.30	0.302	-	0.362	0.362	24.5	25.4	1.48	probe
[15]	Cylindrical	10	0.63	0.154	0.204	-	-	10.4	8.5	1.56	patch
Proposed	Cylindrical	6.85	1.09	0.127	0.39	-	-	13.7	8	5.6	slot

the proposed slots-fed method is not limited by the height of the DRA, so it is very suitable for exciting the low-height DRA. Secondly, the proposed DRA is compared with other omnidirectional CP DRAs in Table 1. Compared with the reported work [8]–[15], our design enjoys a lower height of 0.127 λ_0 and a higher antenna gain of 5.6 dBic. In addition, the size, impedance bandwidth and AR bandwidth of the proposed design are at a medium level. However, the cost of the low-height makes our DRA relatively fat, which has a larger radius of $0.39\lambda_0$. In addition, although the proposed DRA is more easier to fabricate than other work using probe-fed method [8]–[14], the disadvantage is that a printed 4-way power divider is needed.

IV. CONCLUSION

This paper has investigated a slots-coupled omnidirectional CP cylindrical glass DRA. The $TM_{01\delta}$ and $TE_{011+\delta}$ modes of the cylindrical DRA have been applied. It has been found that omnidirectional CP fields are generated as the fields of the two modes are equal in amplitude and 90 degrees phase difference. Compared with the reported omnidirectional CP DRAs, the proposed DRA is easier to fabricate, without introducing supplemental techniques. Also, no hole-drilling is needed for the DRA fabrication. For the demonstration, an omnidirectional CP cylindrical glass DRA has been designed to cover WLAN 5.8-GHz band. It has been found that the proposed glass DRA has a low height of $\sim 0.127\lambda_0$, which can provide an AR bandwidth of $\sim$8 % and a peak gain of $\sim$5.6 dBic. The cost of the proposed design is that a 4-way power divider is required.

APPENDIX

In [21], the resonant modes of the cylindrical DRA are studied. The $TM_{01\delta}$-mode resonance frequency (f_1) of the cylindrical DRA can be estimated using the following formula:

$$f_1 = \frac{c\sqrt{(3.83)^2 + (\frac{\pi R}{2H})^2}}{2\pi R\sqrt{\varepsilon_r}} \tag{A1}$$

While the $TE_{011+\delta}$ mode resonance frequency (f_2) of the cylindrical DRA can be estimated using the following formula:

$$f_2 = \frac{2.208c}{2\pi R\sqrt{\varepsilon_r + 1}}\left[1 + 0.7013\left(\frac{R}{H} - 2.713 \times 10^{-3}(\frac{R}{H})^2\right)\right] \tag{A2}$$

where R, H and ε_r are the radius, height and dielectric constant of the cylindrical DRA, respectively. c denotes the speed of light in vacuum.

REFERENCES

[1] S. Long, M. McAllister, and L. Shen, "The resonant cylindrical dielectric cavity antenna," *IEEE Trans. Antennas Propag.*, vol. 31, no. 3, pp. 406–412, May 1983.
[2] K. M. Luk and K. W. Leung, *Dielectric Resonator Antennas*. Baldock, U.K.: Research Studies Press, 2003.
[3] A. Petosa, *Dielectric Resonator Antenna Handbook*. Norwood, MA, USA: Artech House, 2007.
[4] A. Petosa and A. Ittipiboon, "Dielectric resonator antennas: A historical review and the current state of the art," *IEEE Antennas Propag. Mag.*, vol. 52, no. 5, pp. 91–116, Oct. 2010.
[5] N. Yang, K. W. Leung, and E. H. Lim, "Mirror-integrated dielectric resonator antenna," *IEEE Trans. Antennas Propag.*, vol. 62, no. 1, pp. 27–32, Jan. 2014.
[6] L. Guo, K. W. Leung, S. Q. Wang, and K. F. Tsang, "Investigation of antenna-integrated transparent socket panel," *IEEE Access*, vol. 6, pp. 73001–73008, 2018.
[7] K. W. Leung, X. S. Fang, Y. M. Pan, E. H. Lim, K. M. Luk, and H. P. Chan, "Dual-function radiating glass for antennas and light covers—Part II: Dual-band glass dielectric resonator antennas," *IEEE Trans. Antennas Propag.*, vol. 61, no. 2, pp. 587–597, Feb. 2013.
[8] Y. Mei Pan, K. Wa Leung, and K. Lu, "Omnidirectional linearly and circularly polarized rectangular dielectric resonator antennas," *IEEE Trans. Antennas Propag.*, vol. 60, no. 2, pp. 751–759, Feb. 2012.
[9] W. W. Li and K. W. Leung, "Omnidirectional circularly polarized dielectric resonator antenna with top-loaded alford loop for pattern diversity design," *IEEE Trans. Antennas Propag.*, vol. 61, no. 8, pp. 4246–4256, Aug. 2013.
[10] N. Yang, K. W. Leung, K. Lu, and N. Wu, "Omnidirectional circularly polarized dielectric resonator antenna with logarithmic spiral slots in the ground," *IEEE Trans. Antennas Propag.*, vol. 65, no. 2, pp. 839–844, Feb. 2017.
[11] K. W. Leung, Y. M. Pan, X. S. Fang, E. H. Lim, K.-M. Luk, and H. P. Chan, "Dual-function radiating glass for antennas and light covers—Part I: Omnidirectional glass dielectric resonator antennas," *IEEE Trans. Antennas Propag.*, vol. 61, no. 2, pp. 578–586, Feb. 2013.

[12] M. Khalily, M. R. Kamarudin, M. Mokayef, and M. H. Jamaluddin, "Omnidirectional circularly polarized dielectric resonator antenna for 5.2-GHz WLAN applications," *IEEE Antennas Wireless Propag. Lett.*, vol. 13, pp. 443–446, Mar. 2014.
[13] Y. M. Pan, S. Y. Zheng, and W. Li, "Dual-band and dual-sense omnidirectional circularly polarized antenna," *IEEE Antennas Wireless Propag. Lett.*, vol. 13, pp. 706–709, Apr. 2014.
[14] Y. M. Pan and K. W. Leung, "Wideband omnidirectional circularly polarized dielectric resonator antenna with parasitic strips," *IEEE Trans. Antennas Propag.*, vol. 60, no. 6, pp. 2992–2997, Jun. 2012.
[15] W. Li, K. W. Leung, and N. Yang, "Omnidirectional dielectric resonator antenna with a planar feed for circular polarization diversity design," *IEEE Trans. Antennas Propag.*, vol. 66, no. 3, pp. 1189–1197, Mar. 2018.
[16] M. Yang, Y. Pan, and W. Yang, "A singly fed wideband circularly polarized dielectric resonator antenna," *IEEE Antennas Wireless Propag. Lett.*, vol. 17, no. 8, pp. 1515–1518, Aug. 2018.
[17] M. Zhang, B. Li, and X. Lv, "Cross-Slot-Coupled wide dual-band circularly polarized rectangular dielectric resonator antenna," *IEEE Antennas Wireless Propag. Lett.*, vol. 13, pp. 532–535, Mar. 2014.
[18] M. Zou, J. Pan, Z. Nie, and P. Li, "A wideband circularly polarized rectangular dielectric resonator antenna excited by a lumped resistively loaded Monofilar-Spiral-Slot," *IEEE Antennas Wireless Propag. Lett.*, vol. 12, pp. 1646–1649, Dec. 2013.
[19] S.-L.-S. Yang, A. A. Kishk, and K.-F. Lee, "Wideband circularly polarized antenna with L-Shaped slot," *IEEE Trans. Antennas Propag.*, vol. 56, no. 6, pp. 1780–1783, Jun. 2008.
[20] K. W. Leung, W. C. Wong, and H. K. Ng, "Circularly polarized slot-coupled dielectric resonator antenna with a parasitic patch," *IEEE Antennas Wireless Propag. Lett.*, vol. 1, pp. 57–59, 2002.
[21] R. K. Mongia and P. Bhartia, "Dielectric resonator antennas—A review and general design relations for resonant frequency and bandwidth," *Int. J. Microw. Millim.-Wave Comput.-Aided Eng.*, vol. 4, no. 3, pp. 230–247, Jul. 1994.

XIAO SHENG FANG (Member, IEEE) received the B.Eng. degree in electronic engineering from Sun Yat-sen University, Guangzhou, China, in 2008, and the Ph.D. degree in electronic engineering from The City University of Hong Kong, Hong Kong, in 2012. From 2012 to 2015, he was a Senior Research Assistant with the Department of Electronic Engineering, The City University of Hong Kong. He is currently an Associate Professor with the Department of Electronic Engineering, Shantou University, Shantou, China. His research interests include microwave antennas, dielectric resonator antennas, and passive RF components. He serves as a Technical Reviewer for the IEEE TRANSACTIONS ON ANTENNAS AND PROPAGATION, the IEEE ANTENNAS AND WIRELESS PROPAGATION LETTERS, and IEEE ACCESS.

LING PENG WENG (Graduate Student Member, IEEE) was born in Fuzhou, Fujian, China, in 1995. He received the B.E. degree in electronics and information engineering from Huaqiao University, in 2017. He is currently pursuing the master's degree in engineering with Shantou University. His research interests include dielectric resonator antennas, microwave antennas, and wireless communication.

YU-XIANG SUN (Member, IEEE) was born in Yingcheng, Hubei, China, in November 1987. He received the B.Eng. degree in electronic information science and technology and the M.Sc. degree in radio physics from Wuhan University, Wuhan, China, in 2010 and 2012, respectively, and the Ph.D. degree in electronic engineering from The City University of Hong Kong, Hong Kong, China, in 2016.

From August 2012 to July 2013 and from October 2016 to February 2019, he was a Research Assistant and a Postdoctoral Fellow with The City University of Hong Kong. He joined the College of Electronics and Information Engineering, Shenzhen University, as an Assistant Professor, in March 2019. His current research interests include dielectric resonator antennas (DRA), millimeter-wave antennas, and circularly-polarized antennas.

Dr. Sun serves as a Technical Reviewer for the IEEE TRANSACTIONS ON ANTENNAS AND PROPAGATION, the IEEE ANTENNAS AND WIRELESS PROPAGATION LETTERS, and *IET Microwaves, Antennas and Propagation*.